# Optical-optical double resonance photoionization spectroscopy of *nf* Rydberg states of nitric oxide

Runchuan Zhao, Ian M. Konen,[a] and Richard N. Zare
*Department of Chemistry, Stanford University, Stanford, California 94305*

(Received 21 June 2004; accepted 25 August 2004)

The spectra of vibrationally excited $nf$ Rydberg states of nitric oxide were recorded by monitoring the photoion current produced using two-photon double resonance excitation via the NO $A\,^2\Sigma^+$ state followed by photoexcitation of the Rydberg state that undergoes autoionization. The optical transition intensities from NO $A$ state to $nf$ Rydberg states were calculated, and the results agree closely with experiment. These results combined with circular dichroism measurements allow us to assign rotational quantum numbers to the $nf$ Rydberg states even in a spectrum of relatively low resolution. We report the positions of these $nf(v,N,N_c)$ Rydberg levels converging to the NO $X\,^1\Sigma^+$ $v^+=1$ and 2 ionization limits where $N$ is the total angular momentum excluding electron and nuclear spin and $N_c$ represents the rotational quantum number of the ion core. Our two-color optical-optical double resonance measurements cover the range of $N$ from 15 to 28, $N_c$ from 14 to 29, and the principal quantum number $n$ from 9 to 21. The electrostatic interaction between the Rydberg electron and the ion core is used to account for the rotational fine structure and a corresponding model is used to fit the energy levels to obtain the quadrupole moment and polarizability of the $NO^+$ core. Comparison with a multichannel quantum defect theory fit to the same data confirms that the model we use for the electrostatic interaction between the $nf$ Rydberg electron and the ion core of NO well describes the rotational fine structure. © *2004 American Institute of Physics.* [DOI: 10.1063/1.1807373]

## I. INTRODUCTION

The $nf$ Rydberg states of the NO molecule are generally considered to be a hydrogenlike system owing to the weak interaction between the outer Rydberg electron and the $NO^+$ ion core. In this state the outer electron occupies a hydrogenic orbital with high principal quantum number $n$ while the $NO^+$ ion core is described as a $^1\Sigma^+$ electronic state with a vibrational quantum number $v$ and a rotational quantum number $N_c$. The total angular momentum of the $nf$ Rydberg state is denoted by $N$ (where electron and nuclear spins are ignored). The $f$ Rydberg electron can seldom penetrate into the ion core because of its high centrifugal potential barrier.

Since Jungen and Miescher[1] published the structure of 4,5$f$ Rydberg states in 1969, the $nf$ Rydberg spectra have been studied extensively.[2–7] Various spectroscopic techniques were employed in these experiments to access different Rydberg states and to measure the positions and widths of these states and to determine their transition intensities. Among them, the optical-optical double resonance[2] (OODR) multiphoton ionization (MPI) method offers the opportunity to study a large number of $nf$ Rydberg states. Using this method, data for the $nf$ Rydberg states of different $N_c$, $v$, and $n$ have gradually accumulated. In theoretical studies, Jungen and Miescher[1] developed a model based on the multipole interaction between the ion core and the Rydberg electron with large orbital angular momentum to explain the structure of the $f$ Rydberg states. Eyler and Pipkin[8] improved the form of the multipole interaction model, in which the ion-core rotation is also treated quantum mechanically. Biernacki *et al.*[4] successfully used this model to fit the positions of the $nf$ Rydberg states observed with a high-resolution cw laser.

Some researchers have also studied the dynamics of the vibrational autoionization form the $nf$ Rydberg states.[6–13] The most important experiments in this aspect were done by Park *et al.*[11,12,14] They used rotationally resolved photoelectron spectroscopy to observe the final products of the autoionization from the $ns(v=1,N,N_c)$ ($N_c$ is called $N_R^+$ in Refs. 11, 12, and 14), $np(v=1,N,N_c)$, and $nf(v=1,N_c)$ Rydberg states. Their experiments demonstrated that the orbital angular momentum does not remain invariant during the autoionization process.[15,16] In order to obtain rotational resolution, Park *et al.* excited the ion core to high rotational levels, i.e., $N_c>19$, whose spectra are rarely studied. They assigned the $nf$ Rydberg states based on single-channel quantum defect theory and did multichannel quantum detect theory (MQDT) analysis only on a few particular states. Moreover, their laser resolution was not sufficiently high to resolve the rotational fine structure (energy level splittings caused by $N_c$-$l$ coupling, i.e., $N$) of the $nf(v,N_c)$ Rydberg states. Hence, their photoelectron spectra were unable to determine how an individual $nf(v,N,N_c)$ Rydberg level decays.

The present work explores the OODR-MPI spectra of the NO $nf$ $v=1$ and 2 Rydberg states with high ion-core rotational quantum numbers ($14<N_c<29$). We refined the method to calculate the line intensities to $nf$ Rydberg levels.

[a]Present address: Department of Chemistry, University of Pennsylvania, 231 South 34th Street, Philadelphia, PA 19104-6323.

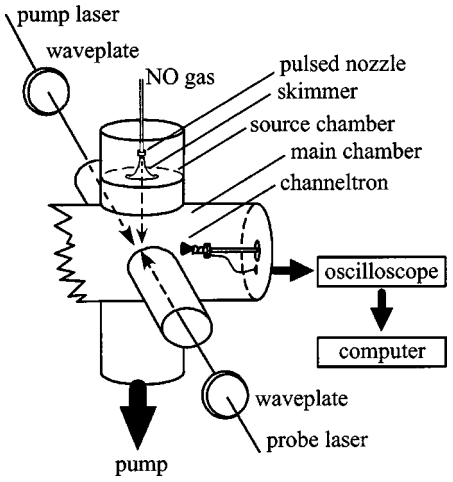


FIG. 1. Schematic diagram of experimental apparatus.

Aided with circular dichroism measurements,[17] we determined the relative intensities of the transitions to the $nf(v,N,N_c)$ Rydberg levels excited by OODR via the NO $A$ state. These intensity measurements permit us to assign unambiguously the $nf(v,N,N_c)$ Rydberg levels. Using these assignments, the energy levels are fit to the multipole-interaction model,[8] from which we obtain values of the quadrupole moment and polarizability of the $NO^+$ ion. For comparison purposes, we also fit the energy levels using multichannel quantum defect theory and the quantum defects are obtained. Both fits are able to reproduce the energy levels of $nf$ Rydberg states we observed. In this manner we are able to explain completely the $nf$ Rydberg spectra obtained by OODR-MPI. Even though the laser's resolution is not adequate to resolve fully the rotational fine structure, our double resonance excitation geometry can reveal the specific nature of different $nf$ Rydberg levels. This information gives us the opportunity to discover the vibrational autoionization decay dynamics of individual NO $nf$ Rydberg levels.

## II. EXPERIMENT

### A. Recording two-color optical-optical double resonance ionization spectra

The experiment apparatus (shown in Fig. 1) is similar to that used by Park *et al.*[11,12] NO gas is injected into the source chamber through a heated pulsed nozzle (General Valve), which is backed with ~1 atmosphere of 99% pure NO (Matheson CP). After being collimated by a skimmer (with a 0.3 mm pinhole, Beam Dynamics) between the source chamber and the main chamber, NO molecules enter the main chamber where they are ionized. The opening of the nozzle is synchronized with the firing of the laser sources. The open duration can be adjusted to optimize the amount of NO gas in the chamber. Because the experiment described here involves high rotational states, the pulsed nozzle is heated and maintained at a temperature of 75 °C to avoid supersonic cooling of the NO. The pressure in the main chamber is $7\times10^{-8}$ torr when the nozzle is off and less than $2\times10^{-7}$ torr when it is on.

The vibrationally autoionizing $nf$ ($v$=1 or 2) Rydberg states are accessed by two-color double resonance excitation of NO via the $A\,^2\Sigma^+$ ($v$=1 or 2) state. The excitation scheme has been described elsewhere in detail.[2,4,12] The pump laser excites NO from rotational levels in the ground state, NO $X\,^2\Pi\,(v''=0,J'')$, to selected rotational levels in the first excited state, NO $A\,^2\Sigma^+$ ($v'=1$ or 2, $J'$, $N'=J'+1/2$). The wavelength is around 214 nm for the (1,0) band, which is generated by a beta barium borate (BBO) crystal that doubles the frequency output from a tunable dye laser (PDL-3) using Excalite 428. For the (2,0) band, the wavelength is around 204 nm, generated by two BBO crystals that triple the frequency output of the same dye laser using SR610. The probe laser excites the NO from a selected rotational level in the $A$ state to a Rydberg state. Because the NO $A$ state potential energy curve is similar in shape to that of the Rydberg states, the Franck-Condon principle limits this transition to be $\Delta v=0$. The wavelength of the probe laser ranges from 343 nm to 326 nm and is generated by a potassium dihydrogen phosphate (KDP) crystal that doubles the frequency output of another tunable dye laser (PDL-1) that uses a dye mixture of DCM and LDS698. The PDL-3 and PDL-1 dye lasers are pumped by DCR-3 and DCR-1A Nd:(yttrium aluminum garnet) YAG lasers, respectively. Both Nd:YAG lasers fire at a repetition rate of 10 Hz and are synchronized so that the probe laser is delayed ~10 ns relative to the pump laser. Two counterpropagating laser beams are coaxially introduced into the main chamber and are perpendicular to the NO molecular beam. The ionization spectra are obtained by scanning the wavelength of the probe laser while setting the pump laser at specific $R_{21}(J'')$ transitions of the NO $A$-$X$ (1,0) or (2,0) bands. Both laser beams are linearly polarized and have parallel polarizations when spectra are being recorded. In order to ensure reliable energy measurements, the wavelength of the probe laser is calibrated by using etalon fringe patterns and comparing them with positions of three xenon excited-state lines.[18] The wavelength of the pump laser is not calibrated because we do not use this wavelength to calculate the energy levels of the $A$ state. Instead, we calculated these energies from reliable spectroscopic parameters given in the literature.[19]

The $NO^+$ ions produced by the autoionization of NO Rydberg states are collected by a channeltron ion detector (Galileo 4839), which is held at a voltage −1700 V relative to the grounded walls of the chambers. The ion signal in the channeltron is sent to a digital oscilloscope (Tektronix TDS 620), where a resident program measures the intensity and then sends the value to a computer for further analysis. The electric field strength at the ionization point introduced by the channeltron is determined by simulation to be less than 10 V/cm. This field strength is insufficient to perturb by a measurable amount the resonance energies of the Rydberg states we studied.

### B. Assignment of *P*, *Q*, and *R* branches from circular dichroism measurements

Circular dichroism (CD) is used to distinguish members of the $P$, $Q$, and $R$ branches in the probe step. We choose the two laser beams to have "parallel" polarizations. By this we

mean that for linear polarizations both electric vectors are parallel to each other and for circular polarizations the propagation directions of both laser beams are parallel. For this choice we can make an incoherent summation over the magnetic sublevels of the lower state, that is, coherence effects can be ignored. Then for the case of optical-optical double resonance ionization, the intensity of the ion signal can be written as an angular part multiplied by a constant $C$,

$$I(\Delta J_1,\Delta J_2,\mu_1,\mu_2) = C\sum_{M''}\begin{pmatrix} J'' & 1 & J' \\ M'' & \mu_1 & -M' \end{pmatrix}^2\begin{pmatrix} J' & 1 & J \\ M' & \mu_2 & -M \end{pmatrix}^2, \quad J'=J''+\Delta J_1, \quad J=J'+\Delta J_2, \tag{1}$$

where double-primed, primed, and unprimed variables are the quantum numbers of the ground, intermediate, and final state respectively. $\Delta J_1$ and $\Delta J_2$ are the changes of the angular momentum quantum number in the pump and probe steps, respectively. They have values of $-1$, 0, and 1, which corresponds to $P$, $Q$, and $R$ branch, respectively. In Eq. (1) $\mu_1$ and $\mu_2$ are the photon's quantum numbers related to their polarizations. In the CD experiment, we set both pump and probe lasers to be circularly polarized. They either have the same helicity (SH) or have opposite helicity (OH). We measure the ion signal intensity for the lasers with the same helicity and for the lasers with opposite helicity and record the intensity ratio $I_{\mathrm{OH}}/I_{\mathrm{SH}}$. The pump step is always an $R$ branch. Therefore for $P$, $Q$, and $R$ branches in the probe step, respectively, the ratio $I_{\mathrm{OH}}/I_{\mathrm{SH}}$, predicted by calculations are

$$\begin{aligned} P \text{ branch:} \quad & \frac{I_{\mathrm{OH}}}{I_{\mathrm{SH}}}=\frac{2J^2-J}{12J^2+24J+10}\xrightarrow{\text{large } J}\frac{1}{6} \\ & \left(\simeq\frac{1}{7} \text{ for } J \text{ in this work}\right), \\ Q \text{ branch:} \quad & \frac{I_{\mathrm{OH}}}{I_{\mathrm{SH}}}=\frac{3J}{3J+5}\xrightarrow{\text{large } J}1, \\ R \text{ branch:} \quad & \frac{I_{\mathrm{OH}}}{I_{\mathrm{SH}}}=6 \quad \text{all } J. \end{aligned} \tag{2}$$

In our experiment the total angular momentum of the Rydberg states $J$ ranges from 15.5 to 27.5 in the experiment. Hence, the high-$J$ limit is appropriate. Examination of Eq. (2) shows that the $P$, $Q$, and $R$ branches can be easily distinguished by looking for peaks that either grow or shrink by a factor of 6, or remain the same. This conclusion obtains for pure branches and for pure polarization states of the laser beams. For blends between different branches or for impure polarization states or for both, these ratios are reduced, as discussed below.

Both pump and probe lasers are originally linearly polarized. In the pump step for the NO $A$-$X(2,0)$ band, a quarter wave plate (Optics for Research) at 204 nm is used to convert linear polarization into circular polarization. For the NO $A$-$X(1,0)$ band, a variable wave plate (New Focus 5540) is carefully adjusted to perform as a quarter wave plate at 214 nm. In the probe step, another New Focus 5540 is used as a wavelength-tunable quarter wave plate over a range of nearly 15 nm. New Focus 5540 works well as a quarter wave plate in the wavelength range of the probe laser, but not so well at 214 nm. There is always residual ellipticity in the pump laser at 214 nm, which causes the measured growing or shrinking factor to be reduced from 6 to 4.5 for pure $P$ or $R$ branches. Nonetheless, the factor of 4.5 is sufficient to distinguish pure $P$, $Q$, and $R$ branch transitions although it is not qualified for quantitative evaluation as discussed later. But for the pump laser at 204 nm, the quarter wave plate produces very good circular polarization. As a result, we obtained the factor of 6 for pure $P$ and $R$ branches in the spectra terminating on the $v=2$ vibrational manifold of the $nf$ Rydberg states.

## III. THEORY AND CALCULATIONS

### A. Relative intensities of transitions to *nf* Rydberg states

The $nf$ Rydberg states are reached by two-step excitation, i.e., from NO ground state to the $A$ state and then from the $A$ state to the Rydberg states. We first consider the transition probabilities in the second step. Both NO $A\,^2\Sigma^+$ and $nf$ Rydberg states are well described by an outer electron coupled with an ion core in a $^1\Sigma^+$ electronic state. In both cases, $N$ and $l$ are good quantum numbers.[20] The difference between them is that the $A\,^2\Sigma^+$ state follows Hund's case (b) whereas $nf$ Rydberg state follows Hund's case (d) coupling. In Hund's case (b), $\lambda$ and $\Lambda$, the projections of $l$ and $N$ onto the internuclear axis, respectively, are good quantum numbers whereas in Hund's case (d), $N_c$ is the good quantum besides $l$ and $N$. In 1983, Cheung *et al.*[2] calculated transition probabilities for the NO $nf$-$A\,^2\Sigma^+$ band system in their experiment. Their calculation was based on the assumption that the $A\,^2\Sigma^+$ state (which consists mainly of $3s\sigma$ character) possesses a small amount of $d\sigma$ character, which makes the $nf$-$A\,^2\Sigma^+$ transition not equal to zero. Their calculational process was to evaluate the electronic dipole moment matrix elements using a Hund's case (a) basis set first and then transform them into case (b) and then into case (d). But in fact it is unnecessary to calculate the electronic dipole moment in a case (a) basis set because the transition does not flip the spin of the electron and no states in Hund's case (a) are involved. Therefore we directly calculate the electronic dipole moment operator matrix between Hund's case (b) basis-set wave functions first and then transform it into Hund's case (d).

The wave function of the NO $A\,^2\Sigma^+$ state, if we consider $d\sigma$ character, can be written as[20]

$$|nd\sigma^+ NM\rangle = |v\Sigma^+\rangle|N,\Lambda=0,M\rangle|nd\sigma\rangle, \tag{3}$$

where $|v\Sigma^+\rangle$ is the vibronic wave function of the $NO^+$ ion core. In Eq. (3) $M$ is the magnetic quantum number associated with $N$. The superscript $+$ sign on $d\sigma$ indicates that the wave function is unchanged upon reflection in a plane containing the internuclear axis. The wave function of NO $nf$ Rydberg state is not an eigenfunction of Hund's case (b). If expanded in a Hund's case (b) basis set, it has the form

$$|nf^{\pm}N_cNM\rangle=\sum_{\lambda}\langle nf\lambda^{\pm}NM|nf^{\pm}N_cNM\rangle|nf\lambda^{\pm}NM\rangle, \tag{4a}$$

$$|nf\lambda^{\pm}NM\rangle=\frac{1}{\sqrt{2(1+\delta_{\lambda 0})}}|v\Sigma^{+}\rangle[|N,\lambda,M\rangle|nf,\lambda\rangle \pm|N,-\lambda,M\rangle|nf,-\lambda\rangle], \tag{4b}$$

where $\langle nf\lambda^{\pm}NM|nf^{\pm}N_cNM\rangle$ is the unitary transformation matrix connecting Hund's case (b) to Hund's case (d), whose form can be found in Ref. 20. As in Eq. (3), we use a superscript $\pm$ sign to indicate electronic reflection symmetry but it is not an independent quantum number. In our case, $N_c+l-N=$even is associated with $\Lambda^{+}$ symmetry and $N_c+l-N=$odd is associated with $\Lambda^{-}$ symmetry.

With excitation by linearly polarized light, the electronic dipole moment between the Hund's case (b) components of the $nf$ Rydberg state and the $A$ state takes the form

$$\begin{aligned}&\langle nf\lambda^{\pm}NM|\mu_z|n'd\sigma^{+}N'M'\rangle\\&=\langle nf\lambda^{\pm},N,\Lambda=\lambda,M|\sum_{q=-1}^{1}D_{0q}^{1*}\mu_q^1\\&\quad\times|n'd\sigma^{+},N',\Lambda'=0,M'\rangle\\&=\text{Const.}\sqrt{(2N+1)(2N'+1)}\begin{pmatrix}2&1&3\\0&\lambda&-\lambda\end{pmatrix}\\&\quad\times\begin{pmatrix}N'&1&N\\0&-\lambda&\lambda\end{pmatrix}(1\mp(-)^{N+N'}),\end{aligned} \tag{5}$$

where the dipole operator $\mu_z$ in lab frame is transformed into molecular frame first.[21] Hence, the electronic dipole moment between an $nf$ Rydberg level in Hund's case (d) and an $A$ state in Hund's case (b) can be obtained by combining Eqs. (4a) and (5).

The relative line intensity of a transition from a level in the $A$ state to the Rydberg level in the OODR spectra is also dependent on the first step, i.e., the excitation from the NO ground state to the $A$ state by the pump laser. Here, we only consider a common excitation geometry: the pump laser is linearly polarized and the polarization is parallel to that of the probe laser. In this case, the line intensity to an $nf$ Rydberg level takes the form

$$\begin{aligned}&I(X\,^2\Pi\rightarrow A\,^2\Sigma^{+}\rightarrow nfN_cN)\\&=\text{Const.}\sum_{M,M'}\langle fN_cNM|\mu_z|d\sigma^{+}N'M'\rangle^2\rho_{M'M'}^{N'},\end{aligned} \tag{6}$$

where $\rho_{M'M'}^{N'}$ is the density matrix of $A\,^2\Sigma^{+}$ state. Assuming that the molecules are unpolarized in their ground states, the $\rho_{M'M'}^{N'}$ has a simple form

$$\rho_{M'M'}^{N'}\propto\begin{pmatrix}N'-\Delta J&1&N'\\-M'&0&M'\end{pmatrix}^2, \tag{7}$$

which is the approximation of a more complicated form[22] when $N'$ is large compared to unity. In Eq. (7) $\Delta J=-1$, 0, or $+1$ if the $A$ state is prepared via $P$-, $Q$-, or $R$-branch transitions, respectively.

What we measure in our experiment is the ion yield, which not only depends on the population of the Rydberg level but also on the competition between autoionization and other decay ways such as predissociation that is not included in our relative line intensity calculation. We discuss this issue in more detail in Sec. III.

### B. Circular dichroism study on branch ratios

Consider the case that a blended line occurs in an OODR spectrum excited by two linear polarized lasers of parallel polarization. This blend includes either three transitions belonging to the $P$, $Q$, and $R$ branches, or two transitions belonging to different branches. Then the CD method can, in the first case, estimate the branch ratio of the strongest transition among the three, and in the second case, give the branch ratios of those two transitions. Recall that the OODR spectra were taken via consecutive excitations by two lasers with parallel and linear polarizations. If we assume $I_R$, $I_P$, and $I_Q$ are the ion intensity of the $R$-, $P$-, and $Q$-branch transitions (again, the pump step is always by means of an $R$ branch) excited by two lasers with parallel and linear polarizations, we have the following relations:

$$\begin{aligned}&P\text{ and }R\text{ branches overlapped:}\quad\frac{I_P}{I_R}\approx\frac{1.5-0.25r}{1.5r-0.22},\\&P\text{ and }Q\text{ branches overlapped:}\quad\frac{I_P}{I_Q}\approx\frac{1.5-1.63r}{1.5r-0.22},\\&R\text{ and }Q\text{ branches overlapped:}\quad\frac{I_R}{I_Q}=\frac{10r+6rJ-6J}{6J-rJ},\end{aligned} \tag{8}$$

where $r$ is the value of the $I_{\mathrm{OH}}/I_{\mathrm{SH}}$ ratio. The numbers appearing in Eq. (8) are calculated at $J=19.5$ which is a good approximation for $J$ in the range from 16.5 through 27.5 in our experiment. Using this relationship, we can draw curves of $I_{\mathrm{OH}}/I_{\mathrm{SH}}$ and $I_{\mathrm{SH}}/I_{\mathrm{OH}}$ versus the relative distributions at different $P$, $Q$, and $R$ branches combinations (shown in Fig. 2). These curves can be used to resolve blended lines into the ratio of different branch transitions that contributed to the overlap.

### C. Multipole interactions

The rotational fine structure of the NO $nf$ Rydberg states, as Jungen *et al.*[1,23] pointed out, is caused by the quadrupole and polarization interactions between the Rydberg electron and the ion core. Eyler and Pipkin[8] developed a quantum mechanical treatment for multipole interactions between the Rydberg electron and the ion core. Actually, similar interactions between the nuclei and the electrons has been well known for a long time.[24] Under Eyler and Pipkin's treatment, the first-order energy correction arising from the quadrupole interaction can be written as

$$E_Q^{(1)} = -\frac{eQ_{zz}[3C(C+1)-4N_c(N_c+1)l(l+1)]}{n^3a_0^3(2l+3)(l+1)(2l+1)l(2l-1)(2N_c+3)(2N_c-1)},$$
$$C = N(N+1)-N_c(N_c+1)-l(l+1), \tag{9}$$

where $Q_{zz}$ is the $zz$ component of the quadrupole momentum tensor of the $NO^+$ ion and $a_0$ is the Bohr radius. In the literature, $Q_{zz}$ is frequently given in atomic unit. To convert the energy from atomic units to $cm^{-1}$, we set $e=a_0=1$, and multiply Eq. (9) by a quantity equal to two times the Rydberg constant. Similarly, the first-order energy correction for the polarization interaction is

$$E_P^{(1)} = -\frac{2e^2\alpha_0}{a_0^4}\frac{3n^2-l(l+1)}{n^5(2l+3)(l+1)(2l+1)l(2l-1)} - \frac{2e^2\gamma[3n^2-l(l+1)]}{3a_0^4n^5} \times \frac{3C(C+1)-4N_c(N_c+1)l(l+1)}{(2l+3)^2(2l-1)^2(l+1)(2l+1)l(2N_c+3)(2N_c-1)},$$
$$C = N(N+1)-N_c(N_c+1)-l(l+1), \tag{10}$$

where $\alpha_0$ is the isotropic part and $\gamma$ is the anisotropic part of the polarizability.

Clearly the energy corrections arising from quadrupole and polarization interactions are dependent on the $n$, $l$, $N_c$, and $N$ quantum numbers. Therefore, for $l=3$ in our case, each rotational level $N_c$ splits into seven sublevels of $N$. Among them, the energy of $N=N_c+3$ is very close to the energy of $N=N_c-3$. Such near degeneracy also exists for the $N=N_c\pm2$ and $N=N_c\pm1$ levels. Comparing Eq. (9) with Eq. (10) more carefully, we can find that the coefficient associated with $Q_{zz}$ and the coefficient associated with $\gamma$ have exactly the same dependence on $N$ and $N_c$. Considering that in our case, $n\geqslant9$ and $l$ is a constant $(=3)$, the two coefficients also have similar dependences on $n$ and $l$. Therefore, in our experiment $Q_{zz}$ and $\gamma$ are indistinguishable. More seriously, in Eqs. (9) and (10) the value of $C$ is nearly a constant if $N_c$ and $N$ have the same relationship (i.e., $N_c-N$ is constant) no matter how $N_c$ varies from 14 to 23 (in $v=2$ spectra) or from 17 to 29 (in $v=1$ spectra). Considering the near degeneracy we mentioned above, $Q_{zz}$ and $\alpha_0$ are strongly correlated for the levels having the same value of $|N_c-N|$. Therefore, in order to have a meaningful fit, the experimental data points should be taken evenly among the seven sublevels.

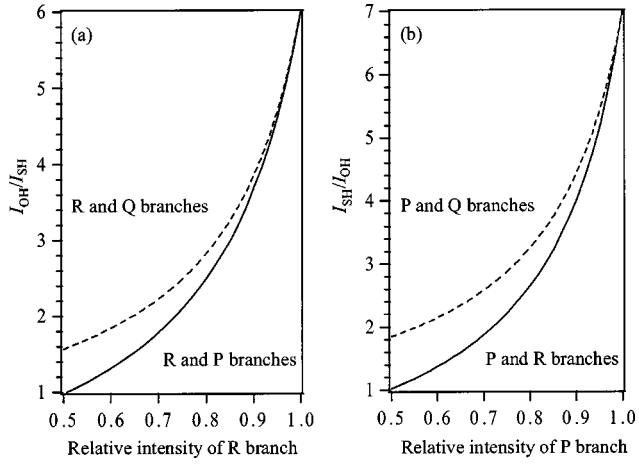


FIG. 2. Circular dichroism measurement used to estimate relative intensity (normalized to one) of a transition in a blended peak: (a) $I_{OH}/I_{SH}$ vs relative intensity of an $R$-branch transition; and (b) $I_{SH}/I_{OH}$ ratio vs relative intensity of a $P$-branch transition. The dashed curves and the solid curves represent the cases when there are only two transitions of different branches as labeled in diagrams. For the cases when there are three transitions belonging to members of the $P$, $Q$, and $R$ branches, respectively, the relative intensities are located between the two curves.

We also fit the energy levels using MQDT. In the MQDT, a number called the quantum defect is used to represent the phase shift imparted to the hydrogenlike wave function. In principle, the quantum defect is the integrated result of all perturbations between the Rydberg electron and the nonhydrogenic ion core. Therefore, by comparing the MQDT fit with the multipole interaction fit, we can examine whether perturbations other than the quadrupole and polarization interactions play significant roles. The full description of MQDT applied to the NO Rydberg states can be found in the literature.[18,25,26] As many researchers[1,12,26,27] have pointed out, there is no $l$ mixing in $nf$ Rydberg states. Hence, it is adequate to consider only seven eigenchannels $f\sigma^+$, $f\pi^\pm$, $f\delta^\pm$, and $f\phi^\pm$ in the fitting procedure.

## IV. RESULTS AND DISCUSSION

### A. OODR-MPI spectra

We recorded $v=1$ spectra terminating in the $v=1$ vibrational manifold of $nf$ Rydberg states via intermediate states $A\,^2\Sigma^+$ $v'=1$ and $N'=19$, 21, 23, and 27. The same was done for and $v=2$ $nf$ Rydberg spectra via $A\,^2\Sigma^+$ $v'=2$, $N'=16$, 17, 18, 19, 20, and 21. Figure 3 presents examples of $v=1$ and $v=2$ spectra. The assignments in the spectra are given by single channel quantum defect theory.[12] The $nf$ Rydberg series associated to $N_c=N'-2$, $N_c=N'$, and $N_c=N'+2$ are found in all spectra. Although allowed by selection rules,[13] $nf$ Rydberg series associated to $N_c=N'\pm4$ are not found except one level $9f$ ($v=2$, $N_c=20$, $N=17$) excited via $A\,^2\Sigma^+$ $v'=2$, $N'=16$ intermediate state. $N_c$-$l$ coupling forms seven $N$ rotational sublevels, but only three

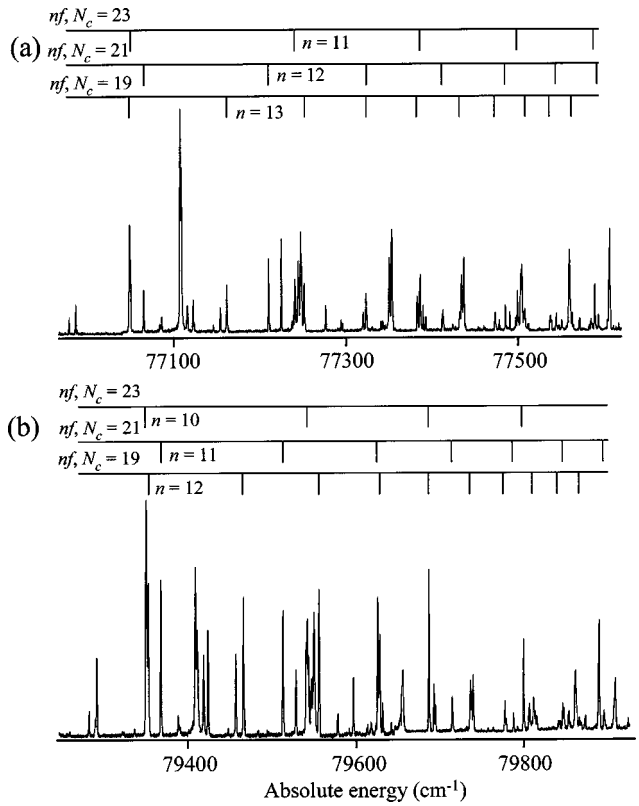


FIG. 3. Examples of OODR-MPI spectra of NO (a) $nf$ ($v$=1) Rydberg states via the intermediate $A\,^2\Sigma^+$ ($v'=1$, $N'=21$, $J'=20.5$) level; and (b) $nf$ ($v$=2) Rydberg states via the intermediate $A\,^2\Sigma^+$ ($v'=2$, $N'=21$, $J'=20.5$) level. The horizontal axis represents the absolute energy relative to the NO ground state $X\,^2\Pi_{1/2}$ ($v''=0$, $J''=1/2$).

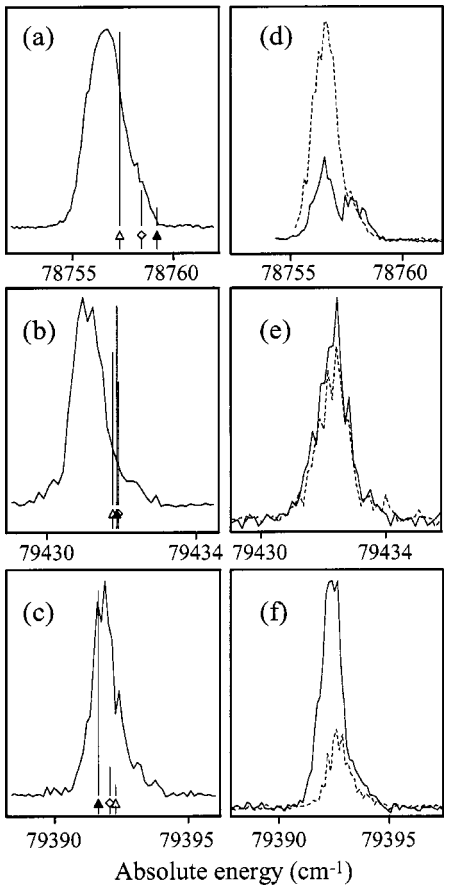


FIG. 4. Circular dichroism study of $nf$ Rydberg collections. Panels (a), (b), and (c) are the $9f$ ($v$=2, $N$=16, 17, and 18, $N_c$=19) collection via the $N'=17$ intermediate state, the $12f$ ($v$=2, $N$=19, 20, and 21, $N_c$=20) collection via the $N'=20$ intermediate state, and the $12f$ ($v$=2, $N$=19, 20, and 21, $N_c$=18) collection via the $N'=20$ intermediate state excited by two counter-propagating linearly polarized laser beams. Three arrows locate the energy positions simulated by the multipole interaction model. △ indicates a *P*-branch transition, ◇ indicates a *Q*-branch transition, and ▲ indicates an *R*-branch transition. The height of the bar right above each arrow represents the calculated line intensity of that transition. Panels (d)–(f) show the corresponding dichroism spectra where the solid line represents excitation by laser beams of opposite helicity and the dashed line represents excitation by laser beams of the same helicity.

of them (belonging to the $N_c=N'\pm2$ and $N'$ series, and corresponding to *P*-, *Q*-, and *R*-branch transitions) can be accessed by our excitation scheme. Our laser source is unable to resolve most of the *N* sublevels. Therefore the $nf$ Rydberg state we observed is what we call a ''collection'' of the three *N* sublevels associated with the same $N_c$ value. The linewidth of an individual $nf$ Rydberg level should be no more than 1 $cm^{-1}$ because the linewidths of the collections are all less than 1 $cm^{-1}$, which is twice that of the linewidth of the probe laser. This observation indicates that the lifetime of an $nf$ Rydberg state is much longer than that of an $np$ Rydberg state, which has a high probability to predissociate.[3,13,16]

### B. Circular dichroism study and line intensity

We studied nearly all $nf$ Rydberg ensembles in the $v$=1 and $v$=2 vibrational manifolds that we could access. Figure 4 presents three of them. Figure 4(a) shows the spectrum connecting to the $9f$ ($v$=2, $N_c$=19) Rydberg ensemble, where $N_c=N'+2$. The arrows under the spectrum locate the energy levels of the $N$=16, 17, and 18 sublevels, which are simulated by multipole interaction fitting. The bars indicate the calculated line intensities. The corresponding CD spectra are shown in Fig. 4(d). Clearly the unresolved spectrum in Fig. 4(a) becomes partially resolved in Fig. 4(d): the left peak in the CD spectra is $N$=16, a *P*-branch transition, which is favored when the two exciting laser beams have the same helicity. The right peak in the CD spectra is either $N$=17 or $N$=18 or both. The overall ensemble performs like a *P* branch with $I_{SH}/I_{OH}$ ratio equal to 4.1, which, according to Fig. 2, means that the *P*-branch transition ($N$=16 level) contributes 91%–93% to the overall peak in Fig. 4(a) and $N$=17 and 18 together only contribute 7%–9%. The calculated branch ratios, as presented in Fig. 4(a), are $N$=16 is 79%, $N$=17 is 14%, and $N$=18 is 7%.

Figure 4(b) shows the spectrum of the $12f$ ($v$=2, $N_c$=20) Rydberg collection where $N_c=N'$. Figure 4(e) is the corresponding CD spectrum which shows that the collection is like a *Q* branch and the measured $I_{OH}/I_{SH}$ ratio is 1.27, just slightly larger than 1.0. So neither $N$=19 (*P* branch) nor $N$=21 (*R* branch) dominates the spectra. But this does not necessarily mean that the *Q* branch dominates the ensemble because no matter how much a real *Q*-branch transition is present in the spectra, if the intensities of *P* branch and *R* branch are equal, then the ensemble should look like a *Q*

TABLE I. Quadrupole moments and polarizabilities. Both quadrupole moment and polarizability are in atomic units. The error bars in this work are given as 90% confidence interval.

| | This work | | Jungen and Lefebvre[a] | Martin *et al.*[b] | Eyler and Biernacki[c] | Biernacki *et al.*[d] |
|---|---|---|---|---|---|---|
| | $v=1$ | $v=2$ | $v=0$ | $v=0$ | $v=3$ | $v=1$ |
| $Q_{zz}(ea_0^2)$ | 0.80(21) | 0.83(23) | 0.58(6) | 0.3052(55) | 0.6894(8) | 0.74(2) |
| $\alpha_0(a_0^2)$ | 8.1(1.1) | 9.0(1.3) | 7.5[e] | 7.7955(12) | 8.182(4) | 8.17(4) |
| $\gamma(a_0^2)$ | $\alpha_0/3$ | $\alpha_0/3$ | $\alpha_0/3$ | 11.578(150) | $\alpha_0/3$ | $\alpha_0/3$ |
| $B$ ($cm^{-1}$) | 1.9680(5) | 1.9492(8) | 1.886[e] | 1.987 946 34[e] | 1.9296(7) | 1.968(2) |

[a]Reference 23. Their value was given in the frame of center of charge of the $NO^+$ ion core. Others (including ours) are given in the center of mass. The data of Ref. 23 refer to $^{14}N^{18}O$.
[b]Reference 32. They gave seven groups of parameters based on different models. We only cite one here.
[c]Reference 5.
[d]Reference 3. The error bars in this column are not confidence intervals.
[e]Fixed.

branch. The calculated branch ratios, as shown in Fig. 4(b), are $N=19$ is 33%, $N=20$ is 25%, and $N=21$ is 42%. For this distribution, the predicted $I_{OH}/I_{SH}$ ratio is 1.1, which is very close to the observed value.

Figure 4(c) shows the $12f$ ($v=2$, $N_c=18$) collection where $N_c=N'-2$. This time, as shown in the CD spectrum in Fig. 4(f), the $N=21$ ($R$ branch) dominates and the measured $I_{OH}/I_{SH}$ ratio is 3.3. According to Fig. 2, the $N=21$ level contributes approximately from 85.6 to 87.4% to the overall intensity of the collection. The branch ratios are calculated to be 4.2% for $N=19$, 11.5% for $N=20$, and 84.3% for $N=21$. This result agrees very well with our observations. Unlike the CD spectra in Fig. 4(d), we do not explicitly observe two or more peaks in Fig. 4(f) owing to the laser's poor resolving power. Nevertheless, it is obvious that the CD spectra are asymmetric about the highest point. The left side of the ensemble prefers the OH excitation so the $N=21$ level should be on the left side. The collection has a long tail to the right side with only a slight helicity preference because according to the calculations $N=20$ is more than two times stronger than $N=19$.

The other $nf$ ($v=2$) Rydberg states, categorized into $N_c=N'+2$, $N_c=N'$, and $N_c=N'-2$, have similar appearance as the above three Rydberg collections, respectively, except for slightly smaller or larger $I_{OH}/I_{SH}$ (or $I_{SH}/I_{OH}$) ratios. Therefore, in our OODR-MPI spectra, the $nf$ ($v=2$, $N=N_c-3$, $N_c$) Rydberg level is dominant (generally $>85\%$) in the $N_c=N'+2$ Rydberg collection and the $nf$ ($v=2$, $N=N_c+3$, $N_c$) Rydberg level is dominant (generally $>85\%$) in the $N_c=N'-2$ Rydberg collection. In many cases, the branch ratios of these levels are so large that the corresponding collections can be considered as pure individual levels. This behavior is caused by the excitation scheme and geometry. For $N_c=N'\pm4$, as mentioned previously, only $9f$ ($v=2$, $N=17$, $N_c=20$) is found and the transition to it is very weak. Our calculations show transitions connecting to $N_c=N'\pm4$ are strictly forbidden, under the assumption that $d\sigma$ character in the $A$ state is the only term permitting transitions to the $nf$ Rydberg states. Therefore, it is not surprising that we can hardly observe the $N_c=N'\pm4$ Rydberg levels. The explanation for the only exception is not well established so far but an argument on a similar phenomenon can be found in Ref. 2. The $v=1$ $nf$ Rydberg states behave similar to $v=2$ $nf$ Rydberg states in the CD spectra. We find, however, that the $I_{OH}/I_{SH}$ and $I_{SH}/I_{OH}$ ratios are noticeably smaller for the $N_c=N'-2$ and $N_c=N'+2$ ensembles whereas $I_{OH}/I_{SH}$ ratio is still very close to one for the $N_c=N'$ ensembles. One apparent explanation for this behavior is the lack of purity of the circular polarization of the laser beam for the $A$-$X(1,0)$ band transitions.

An additional possible explanation is discussed in what follows. Recall that we detect ion yield, whose intensities are not only dependent on the $(1+1')$ transitions probability via the $A$ state but are also dependent on the competition between vibrational autoionization and predissociation of the Rydberg states. Our calculation does not take into account the autoionization-predissociation competition. The very good agreement between the CD measurements and calculations indicates that, for those $nf$ ($v=2$) Rydberg states, either the predissociation probabilities (no matter large or small) are similar for all three $N$ sublevels in an $N_c$ collection, or predissociation is so small compared with autoionization that nearly all molecules excited into these Rydberg states decay into $NO^+$ ions. This conclusion appears contrary to that reported by Fujii and Morita.[10] They found that the decay process in the $7f$ ($v=1$) state is mainly governed by predissociation, and decay rates from the levels of $\Lambda^+$ symmetry (corresponding to $R$- and $P$-branch transitions in our experiment) are much faster than those from the levels of $\Lambda^-$ symmetry (corresponding to $Q$-branch transitions in our experiment). Two possible explanations may account for this seeming disagreement. One is that Fujii and Morita studied low $N_c$ states ($N_c\leqslant3$) whereas we study high $N_c$ states ($N_c\geqslant14$). Low and high $N_c$ states may have different predissociation/autoionization ratios. The other, maybe less significant than previous one, is that different vibrational states could also have different predissociation rates. The $nf$ Rydberg states of $\Lambda^+$ symmetry may experience more predissociation in $v=1$ vibrational state than in $v=2$ vibrational state. This behavior could lead to less $R$- and $P$-branch likeness for $N_c=N'-2$ and $N_c=N'+2$ collections in $v=1$ spectra.

TABLE II. MQDT fitting parameters ($nf$ Rydberg states).

| Quantum defect | This work | | Raoult *et al.*[a] | |
|---|---|---|---|---|
| | $v=1$ | $v=2$ | $7f$ ($v=1$) | $15f$ ($v=1$) |
| $\mu_{f\sigma}$ | 0.0198(62) | 0.0249(112) | 0.0173 | 0.0182 |
| $\mu_{f\pi}$ | 0.0147(56) | 0.0159(103) | 0.0159 | 0.0172 |
| $\mu_{f\delta}$ | 0.0116(52) | 0.0121(99) | 0.0119 | 0.0128 |
| $\mu_{f\phi}$ | 0.0036(66) | 0.0074(68) | 0.0052 | 0.0057 |
| $B$ ($cm^{-1}$) | 1.9678(5) | 1.9493(8) | ··· | ··· |

[a]Reference 26. The rotational constants used are not given in the reference.

### C. Multipole interactions and MQDT

As shown above, the CD spectra reveal the rotational fine structure of the $nf(v,N_c)$ Rydberg collections. As a very good approximation, we can assign in most cases the $N_c=N'\pm 2$ collection in the spectra to an individual Rydberg level $N=N_c\mp 3$. About 80% of the fitting data are from these two kinds of collections. But owing to the correlations in the fit, they cannot provide good fitting just by themselves. Consequently, we also include some data from the $N_c=N'$ collections into the fitting procedure. The $N_c=N'$ collection comprises three individual Rydberg levels of similar intensity. The full width at half maximum (FWHM) of the collection is less than 1 $cm^{-1}$ commonly, and the multipole interaction model indicates the transition to the $N=N_c+1$ level is located in the middle of the collection [see Fig. 4(e)]. Hence it is not a bad approximation to assign the maximum of $N_c=N'$ collection to the $N=N_c+1$ Rydberg level.

With these data, we have the opportunity to go beyond the single-channel quantum defect theory. We use the MQDT method and the multipole interactions to fit the energy levels. This procedure allows us to obtain the quantum defects and the quadrupole moment and polarizability of the NO ion core. This information is generally only available from $nf$ Rydberg states of low principal quantum number[1,5] or by high-resolution laser spectroscopy.[3] We assume that the quantum defects and the multipole moments are different for different vibrational states. Therefore, we fit separately the two vibrational states.

#### 1. Multipole interaction fit

For the multipole interaction, the total perturbed energy is the combination of the quadrupole and polarization interactions given by Eqs. (9) and (10). Because $Q_{zz}$ and $\gamma$ cannot be determined separately by fitting, it is customary to set $\gamma$ equal to a fraction of $\alpha_0$. Jungen and Miescher[1] and Biernacki *et al.*[3,5] used $\gamma=\alpha_0/3$. But the theoretical calculation by Feher and Martin[28] shows $\gamma=\alpha_0/2.13$. Therefore, we try both possibilities. In the range of the principal quantum numbers considered here, the ion level positions are as important as the multipole parameters. These levels (high rotational levels in our experiments) could deviate from their real values significantly if evaluated using inaccurate rotational constants. Therefore, the rotational constants are not fixed but are allowed to vary freely in the fitting. The centrifugal distortion is also included in the calculation to improve the accuracy. The $v=1$ ionization limit of the NO molecule, 77 065.47 $cm^{-1}$, is taken from Ref. 3. The $v=2$ ionization limit of the NO molecule, 77 376.94 $cm^{-1}$, is evaluated from the molecular constants given by Huber and Herzberg[29] and the ionization potential of the NO molecule.[3,30] After fitting, we obtain the multipole parameters and the rotational constants of $NO^+$, which are listed in Table I. If we use $\gamma=\alpha_0/2.13$, we get $Q_{zz}=0.75\pm 0.21$ for $v=1$ and $Q_{zz}=0.78\pm 0.24$ for $v=2$ while $\alpha_0$ and $B$ remain unchanged for both vibrational states. We use the reduced $\chi^2$ value to judge the goodness of the fit.[31] Smaller $\chi^2$ gives a better fit. A rule of thumb is that reduced $\chi^2\approx 1$ indicates a "moderately" good fit. The reduced $\chi^2$ values are always less than 0.7 for both the $v=2$ and $v=1$ data no matter which $\alpha_0/\gamma$ ratio is used. The main reason for such a small reduced $\chi^2$ is that we use the FWHM as the uncertainty in a measured energy level. Owing to the relatively low resolution of the laser and the overlap of some transitions, the FWHMs, whose magnitude are generally 0.3–0.8 $cm^{-1}$ in our experiment, are frequently larger than the rotational fine-structure energy spacings of the sublevels in an $nf$ Rydberg collection. A consequence of

TABLE III. Positions of $nf$ Rydberg states in $v=1$ vibrational manifold and the residuals between calculations and experimental data.

| Rydberg level | | | Measured energy ($cm^{-1}$) | MQDT residual ($cm^{-1}$) | Multipole interaction residual ($cm^{-1}$) |
|---|---|---|---|---|---|
| $n$ | $N_c$ | $N$ | | | |
| 9 | 29 | 26 | 77 414.0 | 0.32 | 0.23 |
| 9 | 29 | 28 | 77 415.2 | −0.22 | −0.32 |
| 10 | 19 | 18 | 76 712.8 | −0.09 | −0.07 |
| 10 | 21 | 18 | 76 872.4 | −0.21 | −0.22 |
| 10 | 21 | 19 | 76 873.2 | −0.25 | −0.09 |
| 10 | 23 | 22 | 77 050.6 | 0.23 | 0.18 |
| 10 | 27 | 28 | 77 450.7 | 0.10 | 0.15 |
| 10 | 29 | 26 | 77 672.6 | 0.17 | 0.10 |
| 10 | 29 | 27 | 77 673.6 | 0.26 | 0.36 |
| 11 | 17 | 20 | 76 757.6 | −0.13 | −0.08 |
| 11 | 21 | 18 | 77 063.7 | −0.26 | −0.25 |
| 11 | 21 | 19 | 77 064.4 | −0.22 | −0.08 |
| 11 | 21 | 23 | 77 064.9 | 0.14 | 0.30 |
| 11 | 21 | 24 | 77 064.2 | 0.20 | 0.24 |
| 11 | 23 | 20 | 77 240.4 | −0.10 | −0.12 |
| 11 | 25 | 22 | 77 432.5 | −0.22 | −0.24 |
| 11 | 25 | 23 | 77 433.3 | −0.08 | 0.00 |
| 11 | 25 | 28 | 77 432.6 | −0.16 | −0.21 |
| 11 | 27 | 26 | 77 641.5 | 0.18 | 0.11 |
| 12 | 21 | 20 | 77 209.9 | −0.15 | −0.17 |
| 12 | 23 | 20 | 77 385.8 | −0.18 | −0.22 |
| 12 | 23 | 22 | 77 386.4 | −0.23 | −0.27 |
| 12 | 23 | 24 | 77 386.7 | −0.04 | −0.07 |
| 12 | 25 | 22 | 77 578.6 | 0.53 | 0.47 |
| 12 | 25 | 28 | 77 578.7 | 0.49 | 0.44 |
| 12 | 29 | 26 | 78 009.6 | −0.30 | 0.30 |
| 13 | 19 | 18 | 77 162.1 | −0.03 | −0.05 |
| 13 | 19 | 22 | 77 161.4 | −0.21 | −0.21 |
| 13 | 21 | 24 | 77 322.6 | 0.02 | 0.00 |
| 13 | 25 | 22 | 77 691.6 | 0.28 | 0.21 |
| 14 | 21 | 24 | 77 412.4 | 0.11 | 0.08 |
| 14 | 23 | 22 | 77 589.2 | −0.09 | −0.16 |
| 15 | 21 | 24 | 77 484.8 | 0.15 | 0.10 |
| 15 | 25 | 28 | 77 853.6 | 0.10 | 0.02 |
| 16 | 19 | 22 | 77 382.6 | −0.33 | −0.37 |
| 20 | 21 | 24 | 77 698.1 | −0.58 | −0.65 |
| 21 | 17 | 20 | 77 417.2 | −0.73 | −0.77 |

TABLE IV. Positions of $nf$ Rydberg levels in $v=2$ vibrational manifold and manifold and the residuals between calculations and experimental data.

| Rydberg level | | | Measured energy ($cm^{-1}$) | MQDT residual ($cm^{-1}$) | Multipole interaction residual ($cm^{-1}$) | Rydberg level | | | Measured energy ($cm^{-1}$) | MQDT residual ($cm^{-1}$) | Multipole interaction residual ($cm^{-1}$) |
|---|---|---|---|---|---|---|---|---|---|---|---|
| $n$ | $N_c$ | $N$ | | | | $n$ | $N_c$ | $N$ | | | |
| 9 | 19 | 16 | 78 756.5 | −0.11 | −0.21 | 12 | 19 | 22 | 79 352.8 | 0.12 | 0.23 |
| 9 | 19 | 17 | 78 758.1 | −0.15 | 0.29 | 12 | 20 | 17 | 79 430.2 | −0.03 | −0.01 |
| 9 | 20 | 17 | 78 834.7 | 0.32 | 0.20 | 12 | 20 | 17 | 79 430.6 | 0.32 | 0.34 |
| 10 | 16 | 17 | 78 806.9 | 0.19 | −0.04 | 12 | 20 | 21 | 79 431.1 | 0.09 | −0.02 |
| 10 | 17 | 18 | 78 872.6 | −0.23 | −0.46 | 12 | 21 | 18 | 79 512.2 | 0.21 | 0.23 |
| 10 | 18 | 15 | 78 941.6 | 0.07 | 0.01 | 12 | 21 | 22 | 79 512.9 | 0.27 | 0.18 |
| 10 | 18 | 17 | 78 942.8 | 0.01 | −0.15 | 12 | 22 | 19 | 79 597.6 | 0.15 | 0.17 |
| 10 | 18 | 19 | 78 943.0 | 0.07 | −0.15 | 12 | 23 | 20 | 79 687.0 | 0.15 | 0.13 |
| 10 | 19 | 16 | 79 015.2 | −0.27 | −0.33 | 13 | 14 | 17 | 79 134.9 | −0.17 | −0.09 |
| 10 | 19 | 20 | 79 017.9 | 0.07 | 0.86 | 13 | 15 | 18 | 79 192.9 | 0.02 | −0.41 |
| 10 | 20 | 17 | 79 093.2 | −0.03 | −0.09 | 13 | 16 | 17 | 79 256.2 | 0.00 | −0.07 |
| 10 | 21 | 18 | 79 175.4 | 0.45 | 0.38 | 13 | 16 | 19 | 79 255.2 | −0.39 | −0.39 |
| 10 | 21 | 22 | 79 176.6 | 0.10 | 0.16 | 13 | 17 | 18 | 79 321.8 | −0.52 | −0.59 |
| 10 | 22 | 19 | 79 260.8 | 0.31 | 0.28 | 13 | 17 | 20 | 79 321.7 | −0.09 | −0.06 |
| 10 | 22 | 20 | 79 261.8 | 0.19 | 0.55 | 13 | 18 | 19 | 79 392.1 | −0.34 | −0.40 |
| 10 | 23 | 20 | 79 350.1 | 0.30 | 0.20 | 13 | 18 | 21 | 79 391.9 | −0.02 | 0.02 |
| 10 | 23 | 20 | 79 349.7 | −0.11 | −0.20 | 13 | 19 | 16 | 79 465.0 | −0.70 | −0.66 |
| 11 | 14 | 17 | 78 876.0 | −0.26 | −0.23 | 13 | 19 | 20 | 79 466.1 | −0.16 | −0.22 |
| 11 | 15 | 18 | 78 934.4 | −0.33 | −0.28 | 13 | 19 | 22 | 79 465.9 | 0.15 | 0.19 |
| 11 | 16 | 17 | 78 997.8 | 0.00 | −0.15 | 13 | 21 | 18 | 79 625.4 | 0.27 | 0.27 |
| 11 | 16 | 19 | 78 996.7 | −0.22 | −0.25 | 13 | 21 | 22 | 79 626.3 | 0.30 | 0.20 |
| 11 | 17 | 18 | 79 063.8 | −0.13 | −0.28 | 14 | 14 | 17 | 79 224.8 | 0.05 | 0.08 |
| 11 | 18 | 15 | 79 132.8 | −0.19 | −0.27 | 14 | 15 | 18 | 79 282.6 | −0.61 | −0.57 |
| 11 | 18 | 19 | 79 134.2 | 0.16 | 0.00 | 14 | 16 | 19 | 79 345.1 | −0.37 | −0.33 |
| 11 | 18 | 19 | 79 134.0 | 0.00 | −0.16 | 14 | 17 | 18 | 79 411.4 | −0.65 | −0.71 |
| 11 | 18 | 21 | 79 133.2 | 0.00 | 0.03 | 14 | 18 | 21 | 79 481.4 | −0.28 | −0.23 |
| 11 | 19 | 16 | 79 206.6 | −0.24 | −0.38 | 14 | 19 | 22 | 79 555.7 | 0.13 | 0.19 |
| 11 | 19 | 22 | 79 207.3 | −0.11 | 0.22 | 15 | 14 | 17 | 79 297.1 | −0.10 | −0.06 |
| 11 | 20 | 21 | 79 286.0 | 0.16 | 0.11 | 15 | 15 | 18 | 79 354.6 | −0.99 | −0.94 |
| 11 | 21 | 18 | 79 366.6 | 0.19 | 0.22 | 15 | 16 | 19 | 79 417.7 | −0.18 | −0.15 |
| 11 | 21 | 22 | 79 367.8 | 0.31 | 0.26 | 15 | 18 | 21 | 79 554.1 | −0.01 | 0.05 |
| 11 | 22 | 19 | 79 452.2 | 0.29 | 0.31 | 15 | 19 | 22 | 79 628.2 | 0.12 | 0.22 |
| 12 | 14 | 17 | 79 021.7 | −0.12 | −0.07 | 16 | 14 | 17 | 79 356.3 | −0.18 | −0.14 |
| 12 | 16 | 17 | 79 143.4 | 0.17 | 0.14 | 16 | 15 | 18 | 79 414.2 | −0.71 | −0.64 |
| 12 | 16 | 19 | 79 141.9 | −0.61 | −0.54 | 16 | 16 | 19 | 79 477.1 | −0.04 | −0.02 |
| 12 | 17 | 18 | 79 209.2 | −0.36 | −0.19 | 16 | 18 | 21 | 79 613.2 | −0.11 | −0.07 |
| 12 | 17 | 20 | 79 207.9 | 0.27 | −0.67 | 17 | 15 | 18 | 79 463.1 | −0.81 | −0.78 |
| 12 | 18 | 15 | 79 278.7 | −0.02 | 0.16 | 17 | 16 | 19 | 79 526.2 | −0.02 | 0.01 |
| 12 | 18 | 19 | 79 278.9 | 0.18 | −0.49 | 17 | 17 | 20 | 79 593.0 | 0.58 | 0.62 |
| 12 | 18 | 21 | 79 278.6 | −0.01 | −0.01 | 17 | 18 | 21 | 79 662.3 | −0.20 | −0.15 |
| 12 | 19 | 20 | 79 353.3 | 0.04 | −0.03 | 18 | 14 | 17 | 79 446.1 | −0.56 | −0.53 |

this procedure is large confidence intervals for the fitted parameters. The correlation between the coefficients of $Q_{zz}$ and $\alpha_0$ in our fitting makes the parameters even more uncertain. These are the reasons that the error bars (90% confidence interval) in this work are larger than those of others in Table I. Among these four sets of parameters from other researchers, three of them were obtained from fits to low $n$ Rydberg levels. Accordingly, they have smaller uncertainties. The error bars for the last one, which were based on $7f$, $12f$, and $15f$ Rydberg states, as mentioned by authors, are not confidence intervals but estimated from variations between fits.[3]

Martin *et al.*[32] and Eyler, Biernacki, and Colson[3,5] added a core-penetration term to the model. They assumed that the $\sigma$ component [in Hund's case (b) coupling] of $nf$ Rydberg states would penetrate to some extent into the core. It is necessary to add this term in low Rydberg states. But for high Rydberg states, this term becomes quite small[3] and we find that fitting with it does not alter the quadrupole moment and the polarizability outside of their error bars. Hence, we do not include it in our final results.

From Table I, we can see that our fitting results for $v=1$ data agree very well with that obtained by Biernacki *et al.*[3] whereas the results for $v=2$ are slightly larger than those of $v=1$. This observation is understandable because at higher vibrational levels, the effective internuclear distance is longer and consequently the multipole effect could be stronger. This explanation seems to be contrary to the comparison between the parameters of $v=2$ and $v=3$ listed in Table I. But remember that the levels in our experiments are high rotational levels whereas the levels in $v=3$ data are low rotational levels. Hence, the comparison between $v=2$ and $v=3$ might not be as meaningful as the comparison between $v=1$ and $v=2$ of our data.

### 2. MQDT fit

Table II lists our results and compares them with those found by other workers. In our fits, the reduced $\chi^2$ values, again, are less than 0.7. Hence, both MQDT and multipole interaction models give good fits. Comparing Tables I and II, we find that the rotational constants produced by fits to these two different models not only agree well with each other for both the $v=1$ and $v=2$ states but also are close to their counterparts calculated from molecular constants of the $NO^+$.[29] In Table II, the quantum defects of $v=1$ state obtained by us are slightly different from those given by Raoult *et al.*[26] This deviation is judged by us to be acceptable when consideration is given to the low resolution of the data. The quantum defects of $v=2$ states are also similar to those of $v=1$ except $\mu_{f\sigma}$, which is significantly larger in the $v=2$ state. The change of $\mu_{f\sigma}$ indicates a slightly stronger Rydberg electron-ion core interaction in the $v=2$ state. This result is consistent with what we find in the multipole interaction fit, i.e., the multipole parameters are bigger in the $v=2$ state than those in the $v=1$ state. Moreover, the $\mu_{f\pi}$, $\mu_{f\delta}$, and $\mu_{f\phi}$ are not found to be significantly changed because the $f\pi$, $f\delta$, $f\phi$ partial waves are always far outside the ion core. Consequently, they can hardly feel the core becoming bigger. In contrast, the $f\sigma$ partial wave has some chance to be close to the ion core and therefore is more sensitive to the change of the size of the ion core.

In Tables III and IV, we give the energy positions of $37f$ Rydberg levels in $v=1$ and 82 levels in $v=2$, respectively. We also list the residuals between the experimental data and the positions simulated by MQDT and the multipole interaction model with the fitted parameters. Looking at these two tables, we find that MQDT and multipole interaction simulations are quite similar. They have similar residuals relative to the measured energy levels. Recall that the multipole interaction model only considers the first-order energy correction arising from quadrupole and polarization interactions whereas the MQDT takes into account their higher-order corrections and also the energy correction arising from perturbations other than quadrupole and polarization interactions. Hence, we conclude that the first-order correction arising from quadrupole and polarization interaction is already sufficient and the presence of other possible perturbations is negligible, given the poor resolving power of our laser sources.

## V. SUMMARY AND CONCLUSIONS

In this study, we have successfully explained $nf$ Rydberg spectra observed by OODR-MRI method. CD measurement proves to be a useful technique to identify $P$, $Q$, and $R$ branch members and to resolve blended lines comprising different branch members. The good agreement between the CD measurement in $v=2$ spectra and the calculations on relative line intensity indicates that the $d\sigma$ character is the major term in $A$ state to permit transitions to $nf$ Rydberg states. It also indicates that the predissociation is either much slower than autoionization or comparable between $\Lambda^+ nf$ Rydberg states and $\Lambda^- nf$ Rydberg state. This behavior is different from that of $nf$ Rydberg states with low rotational quantum number and also slightly different from that of $v=1$ $nf$ Rydberg states whose CD measurements, in some cases, agree less with the calculations. The goodness of the fits obtained by using multipole interaction and by MQDT and the close agreement and consistency between them indicate that the quadrupole and polarization interactions are the dominant perturbations between the $nf$ Rydberg electron and the ion core in NO.

## ACKNOWLEDGMENT

This work is supported by National Science Foundation under Grant No. CHE-0242103.

[1] C. Jungen and E. Miescher, Can. J. Phys. **47**, 1769 (1969).
[2] W. Y. Cheung, W. A. Chupka, S. D. Colson, D. Gauyacq, P. Avouris, and J. J. Wynne, J. Chem. Phys. **78**, 3625 (1983).
[3] D. T. Biernacki, S. D. Colson, and E. E. Eyler, J. Chem. Phys. **89**, 2599 (1988).
[4] D. T. Biernacki, S. D. Colson, and E. E. Eyler, J. Chem. Phys. **88**, 2099 (1988).
[5] E. E. Eyler and D. T. Biernacki, J. Chem. Phys. **88**, 2850 (1988).
[6] E. E. Eyler, W. A. Chupka, S. D. Colson, and D. T. Biernacki, Chem. Phys. Lett. **119**, 177 (1985).
[7] Y. Anezaki, T. Ebata, N. Mikami, and M. Ito, Chem. Phys. **89**, 103 (1984); *ibid.* **97**, 153 (1985); J. Phys. Chem. **87**, 4773 (1983); J. H. Geng, T. Kobayashi, and M. Takami, Chem. Phys. Lett. **266**, 290 (1997); E. F. Mccormack, F. Diteodoro, J. M. Grochocinski, and S. T. Pratt, J. Chem. Phys. **109**, 63 (1998).
[8] E. Eyler and F. Pipkin, Phys. Rev. A **27**, 2462 (1983).
[9] A. Fujii and N. Morita, Chem. Phys. Lett. **182**, 304 (1991); J. Guo, A. Mank, and J. W. Hepburn, Phys. Rev. Lett. **74**, 3584 (1995).
[10] A. Fujii and N. Morita, J. Chem. Phys. **97**, 327 (1992).
[11] H. Park, D. J. Leahy, and R. N. Zare, Phys. Rev. Lett. **76**, 1591 (1996).
[12] H. Park and R. Zare, J. Chem. Phys. **106**, 2239 (1997).
[13] S. T. Pratt, J. Chem. Phys. **108**, 7131 (1998).
[14] H. Park, I. Konen, and R. N. Zare, Phys. Rev. Lett. **84**, 3819 (2000).
[15] E. E. Eyler, Phys. Rev. A **34**, 2881 (1986); C. Jungen, S. T. Pratt, and S. C. Ross, J. Phys. Chem. **99**, 1700 (1995).
[16] A. Giustisuzor and C. Jungen, J. Chem. Phys. **80**, 986 (1984).
[17] I. Konen, R. C. Zhao, and R. N. Zare, in *Dissociative Recombination of Molecular Ions With Electrons*, edited by S. Guberman (Plenum, New York, 2003).
[18] I. Konen, Ph.D., Stanford University, 2002.
[19] V. D. Braun, K. P. Huber, M. Vervloet, C. Amiot, J. Verges, and K. Tsukiyama, J. Mol. Spectrosc. **203**, 65 (2000); J. E. Murphy, B. A. Bushaw, and R. J. Miller, *ibid.* **159**, 217 (1993); C. Amiot and J. Verges, Phys. Scr. **25**, 302 (1982); **26**, 422 (1982).
[20] C. Jungen and G. Raseev, Phys. Rev. A **57**, 2407 (1998).
[21] M. J. Weida and C. S. Parmenter, J. Chem. Phys. **107**, 7138 (1997).
[22] D. Leahy, K. Reid, and R. Zare, J. Chem. Phys. **95**, 1757 (1991); D. Leahy, K. Reid, and R. Zare, J. Phys. Chem. **95**, 8154 (1991).
[23] C. Jungen and H. Lefebvre, J. Mol. Spectrosc. **33**, 520 (1970).
[24] H. B. G. Casimir, *On the Interaction between Atomic Nuclei and Electrons*, 2nd ed. (Freeman, San Francisco, 1963); N. Ramsey, *Nuclear Moments* (Wiley, New York, 1953).
[25] S. Fredin, D. Gauyacq, M. Horani, C. Jungen, G. Lefevre, and F. Masnouseeuws, Mol. Phys. **60**, 825 (1987); C. H. Greene and C. Jungen, ADV Adv. At. Mol. Phys. Phys. **21**, 51 (1985).
[26] M. Raoult, S. Guizard, and D. Gauyacq, J. Chem. Phys. **95**, 8853 (1991).
[27] E. Miescher, Can. J. Phys. **54**, 2074 (1976).
[28] M. Feher and P. A. Martin, Chem. Phys. Lett. **215**, 565 (1993).
[29] K. P. Huber and G. Herzberg, *Constants of Diatomic Molecules* (Van Nostrand Reinhold, New York, 1979).
[30] G. Reiser, W. Habenicht, and K. Mullerdethlefs, Chem. Phys. Lett. **152**, 119 (1988).
[31] W. H. Press, B. P. Flannery, and W. T. Vetterling, *Numerical Recipes* (Cambridge University Press, Cambridge, 1986).
[32] P. A. Martin and P. B. Davies, Can. J. Phys. **72**, 979 (1994).